New constraints on primordial black holes abundance from femtolensing of gamma-ray bursts

A. Barnacka,[1,2,*] J.-F. Glicenstein,[2,†] and R. Moderski[1]

[1]*Nicolaus Copernicus Astronomical Center, Warszawa, Poland*

[2]*DSM/IRFU/SPP, CEA/Saclay, Gif-sur-Yvette F-91191, France*

(Received 6 April 2012; published 2 August 2012)

The abundance of primordial black holes is currently significantly constrained in a wide range of masses. The weakest limits are established for the small mass objects where the small intensity of the associated physical phenomenon provides a challenge for current experiments. We used gamma-ray bursts with known redshifts detected by the Fermi Gamma-ray Burst Monitor (GBM) to search for the femtolensing effects caused by compact objects. The lack of femtolensing detection in the GBM data provides new evidence that primordial black holes in the mass range 10^{17}–10^{20} g do not constitute a major fraction of dark matter.

DOI: 10.1103/PhysRevD.86.043001 PACS numbers: 98.70.Rz, 95.30.Cq, 95.30.Sf, 98.80.Es

I. INTRODUCTION

Dark matter is one of the main and most challenging open problems in cosmology or particle physics, and a number of candidates for particle dark matter have been proposed over the years [1]. The alternative idea that the missing matter consists of compact astrophysical objects was first proposed in the 1970s [2–4]. An example of such compact objects are primordial black holes (PBHs) created in the very early Universe from matter density perturbations. The abundance of PBH above 10^{15} g is a probe of gravitational collapse and large scale structure theory [5]. In particular, it constrains the gravitational wave background produced from primordial scalar perturbations in the radiation era of the early Universe [6].

Recent advances in experimental astrophysics, especially the launch of the Fermi satellite with its unprecedented sensitivity, have revived the interest in PBH physics [7,8]. One of the most promising ways to search for PBHs is to look for lensing effects caused by these compact objects. Since the Schwarzschild radius of PBH is comparable to the photon wavelength, the wave nature of electromagnetic radiation has to be taken into account. In such a case, lensing caused by PBHs introduces an interferometry pattern in the energy spectrum of the lensed object [9]. The effect is called "femtolensing" [10] due to the $\sim 10^{-15}$ arcseconds angular distance between the images of a source lensed by a 10^{18} g lens. The phenomenon has been a matter of extensive studies in the past [11] but the research was almost entirely theoretical since no case of femtolensing has been detected as yet. Gould [10] first suggested that the femtolensing of gamma-ray bursts (GRBs) at cosmological distances could be used to search for dark matter objects in the mass range 10^{17}–10^{20} g. Femtolensing could also be a signature of another dark matter candidate: clustered axions [12].

*abarnack@camk.edu.pl
†glicens@cea.fr

In this paper, we present the results of a femtolensing search performed on the spectra of GRBs with known redshifts detected by the GBM onboard the Fermi satellite. The nonobservation of femtolensing on these bursts provides new constraints on the PBH's fraction in the mass range 10^{17}–10^{20} g. We describe in details the optical depth derivation based on simulations applied to each burst individually. The sensitivity of the GBM to the femtolensing detection is also calculated.

The paper is organized as follows. In Sec. II the basic equations for femtolensing and the calculation of lensing probability are given. Section III describes the data sample and simulations. In Sec. IV the results are presented, and Sec. V is devoted to discussion and conclusions.

II. FEMTOLENSING

A. Magnification and spectral pattern

Consider a lensing event of a GRB by a compact object. The angular diameter distances from the observer to the lens, from the lens to the GRB source, and from the observer to the source are D_{OL}, D_{LS}, and D_{OS}, respectively [13]. Coordinates are taken in the lens plane. The lens, with mass M, is located at the origin. The source position projected onto the lens plane is given by r_S; the distance between the lens and true source position. The Einstein radius r_E is given by

$$r_E^2 = \frac{4GM}{c^2}\frac{D_{OL}D_{LS}}{D_{OS}} \approx (c \times 0.3\ \mathrm{s})^2\left(\frac{D_{OL}D_{LS}}{D_{OS} 1\ \mathrm{Gpc}}\right)\left(\frac{M}{10^{19}\ \mathrm{g}}\right). \tag{1}$$

The image positions are given as usual by

$$r_\pm = \frac{1}{2}\left(r_S \pm \sqrt{r_S^2 + 4r_E^2}\right). \tag{2}$$

The time delay δt between the two images is given by

$$c\delta t = V(r_+; r_S) - V(r_-; r_S), \tag{3}$$

where $V(r; r_S)$ is the Fermat potential at the position r in the lens plane:

$$V(r; r_S) = \frac{1}{2}\frac{D_{OS}}{D_{LS}D_{OL}}(r - r_s)^2 - \frac{4GM}{c^2}\ln(r). \tag{4}$$

One finds:

$$\frac{c\delta t}{(z_L + 1)} = \frac{1}{2}\left(\frac{D_{OS}}{D_{OL}D_{LS}}\right)(r_-^2 - r_+^2) - \frac{4GM}{c^2}\ln\left(\frac{r_+}{r_-}\right). \tag{5}$$

The phase shift between the two images is

$$\Delta\phi = \frac{E\delta t}{\hbar}, \tag{6}$$

where E is the energy of the photon.

In the case of a point source, the amplitude contributed by the $r_\pm$ images is

$$A_\pm \propto \frac{\exp(i\phi_\pm)}{\sqrt{|1 - \frac{r_E^4}{r_\pm^4}|}}. \tag{7}$$

The magnification A^2 is obtained by summing the amplitudes (7) and squaring, which gives

$$\begin{aligned}|A|^2 &= |A_+ + A_-|^2 \\ &= \frac{1}{1 - \frac{r_E^4}{r_+^4}} + \frac{1}{1 - \frac{r_E^4}{r_-^4}} + \frac{2\cos(\Delta\phi)}{\sqrt{|1 - \frac{r_E^4}{r_+^4}|}\sqrt{|1 - \frac{r_E^4}{r_-^4}|}}.\end{aligned} \tag{8}$$

The energy dependent magnification produces fringes in the energy spectrum of the lensed object.

The size of the expanding GRB and the relative motions of the GRB, the lens and the observer should be, in principle, taken into account. If the GRB is observed at a time $t_{\rm expl}$ after the beginning of the burst, its size projected onto the lens plane is

$$s_{\rm GRB} \approx \frac{D_{OL}}{D_{OS}}\frac{ct_{\rm expl}}{\Gamma} \approx (c \times 0.01\ {\rm s})\left(\frac{t_{\rm expl}}{1\ {\rm s}}\right)\left(\frac{\Gamma}{100}\right)^{-1}\left(\frac{D_{OL}}{D_{OS}}\right), \tag{9}$$

where Γ is the Lorentz factor of the burst. Note that the Lorentz factor of GRBs is estimated to be in excess of 100, so that $s_{\rm GRB}$ given in Eq. (9) is overestimated.

The ratio of $s_{\rm GRB}$ to r_E is therefore

$$\begin{aligned}\frac{s_{\rm GRB}}{r_E} &\approx \frac{c^2}{2G^{1/2}}\frac{t_{\rm expl}}{M^{1/2}\Gamma}\left(\frac{D_{OS}D_{LS}}{D_{OL}}\right)^{-1/2} \\ &\approx 0.03\left(\frac{D_{OS}D_{LS}}{D_{OL}1\ {\rm Gpc}}\right)^{-(1/2)}\left(\frac{t_{\rm expl}}{1\ {\rm s}}\right)\end{aligned} \tag{10}$$

$$\times\left(\frac{\Gamma}{100}\right)^{-1}\left(\frac{M}{10^{19}\ {\rm g}}\right)^{-(1/2)}. \tag{11}$$

Equation (11) shows that the finite size of the GRB can be, in general, safely neglected if $t_{\rm expl} < 10$ s.

The Einstein radius crossing time t_E is given by

$$t_E = \frac{r_E}{v} \approx 300\ {\rm s}\left(\frac{r_E}{c \times 0.3\ {\rm s}}\right)\left(\frac{v}{300\ {\rm km/s}}\right)^{-1}, \tag{12}$$

where v is the projected velocity of the source in the lens plane. Equation (12) shows that $t_E \gg t_{\rm expl}$ under reasonable assumptions on the velocities. If so, the motion of the source in the lens plane can also be neglected. In the analysis of GRB spectra, it is thus assumed that the point source-point lens assumption is valid and that the source stays at a fixed position in the lens plane.

B. Lensing probability

The lensing probability of gamma-ray burst events is calculated in two steps. First, the optical depth τ for lensing by compact objects is calculated according to the formalism of Fukugita *et al.* [14]. The cosmological parameters used in the calculation are: a mean mass density $\Omega_M = 0.3$ and a normalized cosmological constant $\Omega_\Lambda = 0.7$. The calculations are made for both the Friedmann-Lemaître-Robertson-Walker (FLRW) and the Dyer-Roeder [15] cosmology. In our sample, the GRB redshift z_s is known. The lens redshift z_L is assumed to be given by the maximum of the $d\tau/dz_L(z_S)$ distribution (see, e.g., Fig. 5 of [14]). When $\tau \ll 1$, the lensing probability p is given by $p = \tau\sigma$ where σ is the "lensing cross section" (see Chap. 11 of [16]).

In this paper, the cross section is defined in the following way. Fringes are searched in the spectra of GRBs. These fringes are detectable only for certain positions r_S of the source. The exact criteria for detectability will be given in Sec. III C. The maximum and minimum position of r_S in units of r_E are noted $r_{S,\rm min}$ and $r_{S,\rm max}$. They are found by simulation and depend on the GRB redshift and luminosity. A minimum value of r_S occurs because the period of the spectral fringes becomes larger than the GBM energy range at small r_S.

The femtolensing "cross section" is simply

$$\sigma = r_{S,\rm max}^2 - r_{S,\rm min.}^2 \tag{13}$$

The lensing probability does not depend on the individual masses of lenses but only on the density of compact objects Ω_{CO}. In the optical depth calculation, an increase in the mass of the lenses is compensated by a decrease in the number of scatterers. Therefore, the constraints for a given mass depend only on the cross section σ.

III. DATA ANALYSIS

In our analysis, we use a sample of GRBs with known redshifts. The selection of these bursts is described in Sec. III A. Each burst is fitted to a standard spectral model, as explained in Sec. III B. Finally, the sensitivity of each burst to femtolensing is studied with simulated data. The simulation is described in Sec. III C.

A. Data selection

The GBM [17] onboard the Fermi satellite consists of 12 NaI and two BGO scintillators which cover the energy range from 8 keV up to 40 MeV in 128 energy bins. These detectors monitor the entire sky. In the first two years of operation, the GBM triggered on roughly 500 GRBs. In this paper, only the bursts with known redshifts have been investigated. The initial sample consisted of 32 bursts taken from Gruber *et al.* [18] and five additional bursts from the GRB Coordinates Network (GCN) circulars [19].

For 17 bursts the amount of available data was not sufficient to obtain good quality spectra. The final sample thus consists of 20 bursts, which are listed in Table I.

B. Data processing and spectral analysis

The GBM data are publicly available in the CSPEC format and were downloaded from the Fermi FSSC website [20]. The CSPEC files contain the counts in 128 energy channels binned in 1.024 s for all detectors. Only detectors with a minimal signal-to-noise ratio of 5.5 in each bin were selected for the analysis.

Data were analyzed with the RMfit version 33pr7 program. The RMfit software package was originally developed for the time-resolved analysis of BATSE GRB data but has been adapted to GBM and other instruments.

For each detector with sufficient data, the background was subtracted and the counts spectrum of the first 10 seconds of the burst (or less if the burst was shorter) were extracted.

The energy spectrum was obtained with a standard forward-folding algorithm. Several GRB spectral models, such as a BKN, Band's model (BAND), or a SBKN, where considered. The femtolensing effect was added as a separate model. The magnification and the oscillating fridges were calculated according to Eq. (8) and then multiplied with the BKN or BAND functions.

C. Simulations

The detectability of spectral fringes has been studied with simulated signals. The detectability depends firstly on the luminosity and the redshift of the bursts, and secondly on the detector's energy resolution and the data quality. The sensitivity of the GBM to the lens mass M also depends strongly on the energy range and resolution of the GBM detectors. When small masses are considered, the pattern of spectral fringes appears outside of the energy range. The large masses produce fringes with hardly detectable amplitudes and periods smaller than the energy bin size.

TABLE I. The sample of 20 GBM GRBs used in the analysis.

				Fit to simulated data					
		Fit to the data[a]		Model	Femtolensing			Lensing probability	
Name	z_S	Model	χ^2/d.o.f	χ^2/d.o.f.	χ^2/d.o.f.	$r_{S,\max}$	z_L	FRLW[b]	Dyer-Roeder[c]
GBM 080804972	2.2045	BAND	68/74	129/74	80/72	2.5	0.770	0.145	0.145
GBM 080916009C	4.3500	BKN	75/74	115/74	93/72	3	1.087	0.489	0.444
GBM 080916406A	0.6890	BKN	58/57	91/55	67/53	3	0.324	0.031	0.033
GBM 081121858	2.5120	BKN	39/49	63/52	50/50	3	0.829	0.250	0.245
GRB 081222204	2.7000	BKN	73/66	89/62	68/60	3.5	0.859	0.374	0.364
GRB 090102122	1.5470	BAND	81/85	124/85	92/83	3	0.603	0.134	0.127
GRB 090323002	3.5700	BAND	77/77	106/64	95/62	2	0.964	0.173	0.162
GRB 090328401	0.7360	BKN	105/70	124/70	64/68	2.5	0.346	0.024	0.026
GRB 090424592	0.5440	BAND	78/67	215/78	104/76	4	0.256	0.035	0.038
GRB 090510016	0.9030	BKN	62/66	108/98	94/96	1.5	0.406	0.012	0.013
GRB 090618353	0.5400	BAND	59/72	158/69	93/67	3	0.254	0.019	0.021
GRB 090926181	2.1062	BAND	87/81	247/81	123/79	4	0.737	0.348	0.349
GRB 091003191	0.8969	BKN	93/94	140/94	96/92	3	0.400	0.049	0.053
GRB 091020900	1.7100	BKN	74/69	100/69	77/67	3	0.667	0.144	0.147
GRB 091127976	0.4900	BAND	78/74	84/74	71/72	4	0.240	0.029	0.031
GRB 091208410	1.0630	BAND	55/55	101/55	54/53	3	0.457	0.066	0.070
GRB 100414097	1.3680	BKN	65/61	120/68	92/66	2.5	0.560	0.070	0.073
GRB 100814160A	1.4400	BKN	86/70	181/70	110/68	2	0.590	0.049	0.051
GRB 100816009	0.8049	BKN	67/56	83/56	68/54	3	0.360	0.041	0.043
GRB 110731465	2.8300	SBKN	72/64	96/53	78/51	3	0.877	0.292	0.283

[a]Fit has been performed using only the photons arrived in less than 10 s from the beginning of the burst.
[b]For assumed $\Omega_{CO} = 0.0310$.
[c]For assumed $\Omega_{CO} = 0.0336$.

Because the data quality and the background are not easily simulated, the detectability estimation is performed on real data. Namely, GRB events with known redshift are selected. Since the source redshift is known, the lens redshift is assumed to be the maximum value of $d\tau/dz_L(z_S)$ as explained in Sec. II B. Thus, for a given observed GRB, the femtolensing signal only depends on two parameters: the lens mass M and the source position in the lens plane r_S. The data are then processed as follows:

(1) The magnification [Eq. (8)] as a function of the energy is calculated for the given lens mass M and position of the source r_S.

(2) This magnification is then convolved with the instrumental resolution matrix to obtain magnification factors for each channel of the detector.

(3) The spectral signal is extracted from the data by subtracting the background. It is then multiplied by the corrected magnification.

(4) The background is added back.

The detectability calculation can be illustrated with the luminous burst GRB 090424592. The spectral data of this burst were first fitted with standard spectral models: BKN, SBKN, and BAND. The GRB 090424952 burst is best fitted with the BAND model. The fit has $\chi^2 = 78$ for 67 d.o.f. The BAND model has four free parameters: the amplitude A, the low energy spectral index α, the high energy spectral index β, and the peak energy $E_{\rm peak}$ [21].

The data are then modified by incorporating the spectral fringe patterns for a range of lens masses M and source positions r_S. The simulated data and the corresponding femtolensing fit are presented in Fig. 1. Neither BKN nor

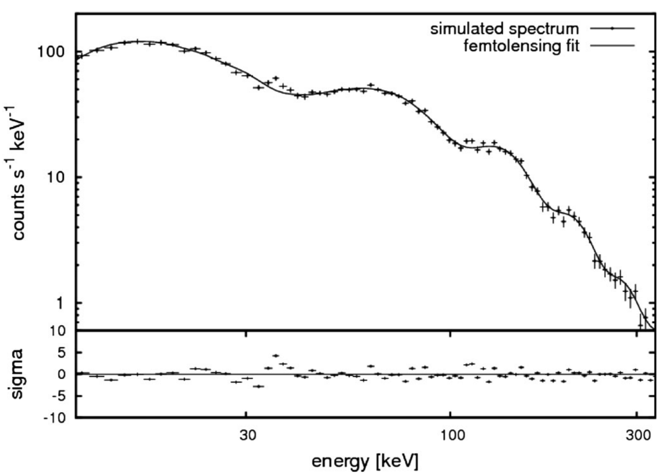

FIG. 1. Simulated spectrum obtained with GRB 090424592. The spectrum was fitted with femtolensing + BAND model. The fit has $\chi^2 = 79$ for 73 d.o.f. The fit parameters are: $A = 0.32 \pm 0.01$ ph s^{-1} cm^{-2} keV^{-1}, $E_{\rm peak} = 179 \pm 3$ keV, $\alpha = -0.87 \pm 0.02$, and $\beta = -3.9 \pm 7.5$. The simulated femtolensing effect is caused by a lens at redshifts $z_L = 0.256$ and a source at $z_S = 0.544$. The simulated mass is $M = 1 \times 10^{18}$ g and the mass reconstructed from the fit is 1.01×10^{18} g. The source is simulated at position $r_S = 2$. The position reconstructed from the fit is $r_S = 1.9$.

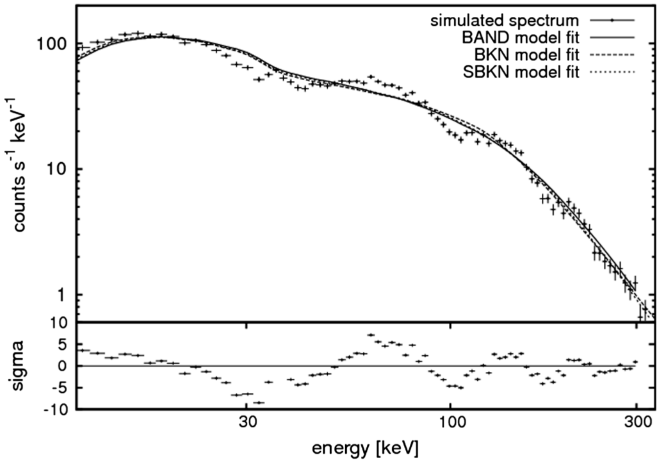

FIG. 2. Simulated femtolensed spectrum fitted with the BAND model. The fit has $\chi^2 = 752$ for 75 d.o.f. The fit parameters are: $A = 0.36 \pm 0.01$ ph s^{-1} cm^{-2} keV^{-1}, $E_{\rm peak} = 174 \pm 5$ keV, $\alpha = -0.8 \pm 0.02$, and $\beta = -2.4 \pm 0.1$. The smoothly broken power law (SBKN) model fit is almost indistinguishable from the broken power law (BKN) model fit.

BAND models are able to fit the simulated data (see Fig. 2). The values of r_S are then changed until the χ^2 of the fit obtained is not significantly different from the χ^2 of the unmodified data. More precisely, the χ^2 difference $\Delta\chi^2$ should be distributed in the large sample limit as an χ^2 distribution with 2 d.o.f. according to Wilk's theorem [22]. The value $\Delta\chi^2 = 5.99$, which corresponds to an χ^2 probability of 5% for 2 d.o.f., was taken as the cut value. The effect of changing r_S on the femtolensing model is illustrated in Figs. 3 and 4.

The pattern in energy is visible when the phase shift between the two images $\Delta\phi \sim (E/1\,{\rm MeV})(M/1.5 \times 10^{17}\,{\rm g})$ is close to 1.

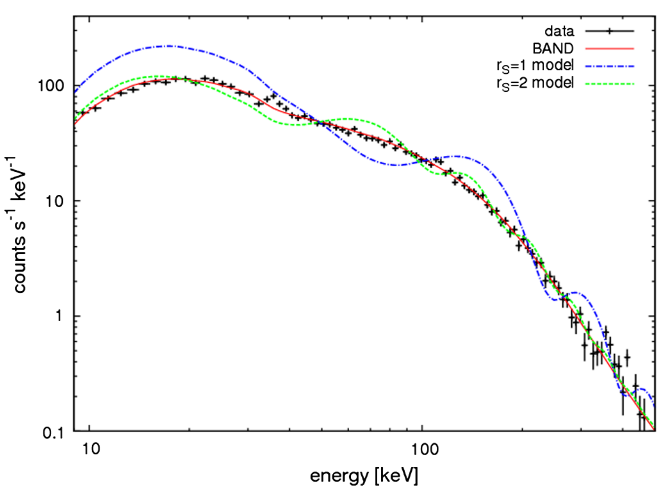

FIG. 3 (color online). The spectrum of GRB 090424592 using NaI detector n7, with the BAND and femtolensing fits superimposed. The parameters are $r_S = 1, 2$, and lens mass 1×10^{18} g. The models are convolved with the response matrix.

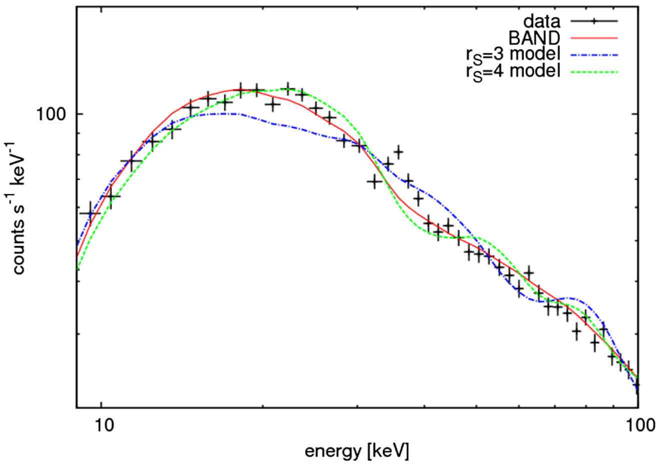

FIG. 4 (color online). The spectrum of GRB 090424592 using NaI detector n7. The BAND and femtolensing fits are superimposed. The parameters are $r_S = 3, 4$, and lens mass 1×10^{18} g. The excess at 33 keV (K edge) is an instrumental effect seen on many bright bursts.

The GBM detector can detect photons with energy from few keV to ~MeV. Lens masses from 10^{17} g to 10^{20} g are thus detectable with GBM. The femtolensing pattern can be detected when the period of the fringes is larger than the detector energy resolution and smaller than the detector energy range. The value of $r_{S,\max}$ comes from the comparison of the period of the oscillating pattern to the detector energy resolution. The value of $r_{S,\min}$ arises from the comparison of the period of the fringes to the detector energy range. Because of these constraints, the most sensitive mass range is 10^{18} g to 10^{19} g.

In Fig. 5 we show the maximum and minimum detectable r_S for different lens masses. The maximum difference between $r_{S,\max}$ and $r_{S,\min}$ appears at $M = 1 \times 10^{18}$ g, which indicates the maximum of femtolensing cross section.

IV. RESULTS

The 20 burst sample from Table I have been fitted with the standard BKN, BAND, and SBKN models. The models with the best χ^2 probability were selected and are shown in Table I. The bursts are well fitted by these standard models, so there is no evidence for femtolensing in the data.

As explained in Sec. II B, the lensing probability for each burst depends on the lens mass and on the $r_{S,\min}$ and $r_{S,\max}$ values. Since the sensitivity of GBM to femtolensing is maximal for lens masses of $\sim 1 \times 10^{18}$ g (see Fig. 5), the values of $r_{S,\min}$ and $r_{S,\max}$ for each event were first determined at a mass $M = 1 \times 10^{18}$ g by simulation. As explained in Sec. II B, the value of $r_{S,\min}$ is set by the period of the spectral fringes so that it is independent of the burst luminosity. The values of $r_{S,\max}$ obtained are listed in Table I. The lensing probability is then calculated for both the FRLW and Dyer-Roeder cosmological models using each burst redshift, the most probable lens position, and the values of $r_{S,\min}$ and $r_{S,\max}$ for the mass $M = 1 \times 10^{18}$ g. The number of expected lensed bursts in the sample is the sum of the lensing probabilities. It depends linearly on Ω_{CO}.

Since no femtolensing is observed, the number of expected events should be less than three at 95% confidence level (C.L.). The constraints on the density of compact objects Ω_{CO} is derived to be less than 4% at 95% C.L. for both cosmological models. The values of the lensing probabilities for all the bursts in our sample assuming the constrained density of compact objects are shown in Table I. The limits at other lens masses are obtained by normalizing the Ω_{CO} at $M = 1 \times 10^{18}$ g by the cross section σ. The cross section is calculated using the Eq. (13), and the values of $r_{S,\min}$ and $r_{S,\max}$ from Fig. 5. The limits on Ω_{CO} at 95% C.L. are plotted in Fig. 6.

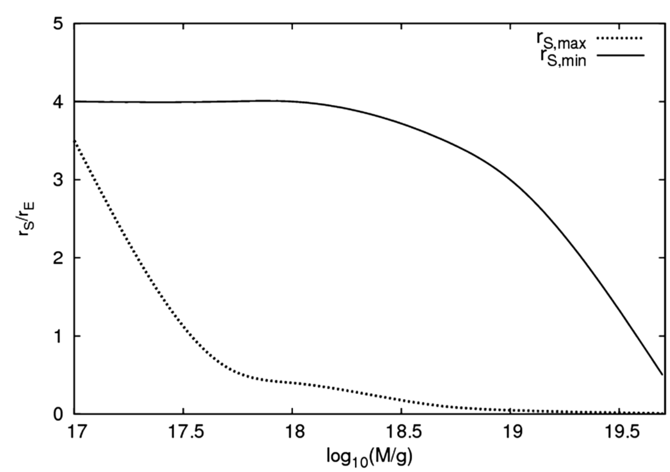

FIG. 5. Minimum and maximum detectable r_S/r_E as a function of lens mass for GRB 090424592.

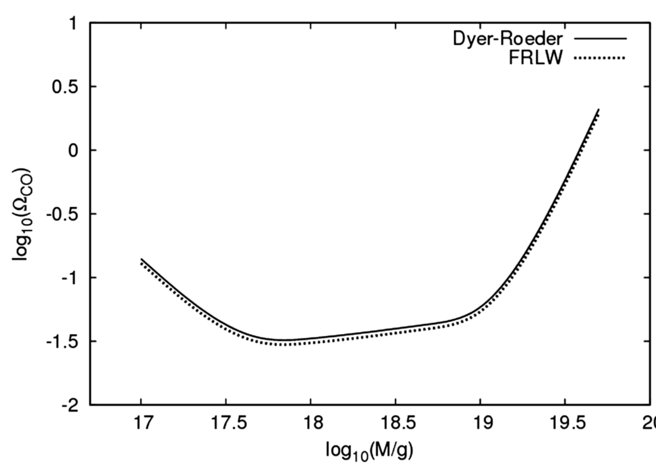

FIG. 6. Constraints on the fraction (or normalize density) of compact objects. The zones above the curves are excluded at the 95% confidence level.

V. DISCUSSION AND CONCLUSIONS

Cosmological constraints on the PBH abundance are reviewed by Carr *et al.* [7]. One way to obtain the abundance of PBH is to constrain the density of compact objects Ω_{CO}. Note that the limits on the compact object abundance in the range of 10^{26}–10^{34} g obtained with microlensing are at the 1% level.

It is stated by Abramowicz *et al.* [23] that the mass range 10^{16} g $< M_{BH} < 10^{26}$ g is virtually unconstrained.

Constraints in the mass range 10^{17} g $< M_{BH} < 10^{20}$ g were given by Marani *et al.* [24]. Their results are based on a sample of 117 bright bursts detected by the BATSE satellite. The bursts were searched for spectral features by Briggs *et al.* [25]. The constraints reported by Marani *et al.* [24] are $\Omega_{CO} < 0.2$ if the average distance to the GRBs is $z_{\rm GRB} \sim 1$ or $\Omega_{CO} < 0.1$ if $z_{\rm GRB} \sim 2$.

Under the mass 5×10^{14} g, the Ω_{CO} is constrained by PBH evaporation. Above the femtolensing range, the constraints come from microlensing. The new idea by Griest *et al.* [8] shows that the microlensing limit could be improved and get constraints down to 10^{20} g with the Kepler satellite observations.

The Fermi satellite was launched three and a half years ago. Since then, almost 1000 of GRB were observed with the GBM detector. In many cases, data quality is good enough to reconstruct time-resolved spectra. This unique feature is exploited in our femtolensing search by selecting the first few seconds of a burst in data analysis.

Our limits were obtained by selecting only those bursts with known redshifts in the GBM data. This reduces the data sample from the 500 bursts detected in the first two years to only 20. The constraints on Ω_{CO} obtained at the 95% C.L. are shown in Fig. 6. These constraints improve the existing constraints by a factor of 4 in the mass range 1×10^{17}–10^{20} g.

After 10 years of operation, the GBM detector should collect over 2500 bursts. Only a few of the bursts, say 100, will have a measured redshift and sufficient spectral coverage. By applying the methods described in this paper, our limits will then improve by a factor of 5, reaching a sensitivity to density of compact objects down to the 1% level.

ACKNOWLEDGMENTS

We would like to thank M. Jaroszyński for useful comments. Part of this research was supported by the Polish Ministry of Science and Higher Education under Grants Nos. DEC-2011/01/N/ST9/06007 and PMN CTA 1891.

[1] J. L. Feng, Annu. Rev. Astron. Astrophys. **48**, 495 (2010).
[2] B. J. Carr and S. W. Hawking, Mon. Not. R. Astron. Soc. **168**, 399 (1974).
[3] S. W. Hawking, Nature (London) **248**, 30 (1974).
[4] S. Hawking, Mon. Not. R. Astron. Soc. **152**, 75 (1971).
[5] B. J. Carr, arXiv:astro-ph/0511743.
[6] E. Bugaev and P. Klimai, Phys. Rev. D **83**, 083521 (2011).
[7] B. J. Carr, K. Kohri, Y. Sendouda, and J. Yokoyama, Phys. Rev. D **81**, 104019 (2010).
[8] K. Griest, M. J. Lehner, A. M. Cieplak, and B. Jain, Phys. Rev. Lett. **107**, 231101 (2011).
[9] A. V. Mandzhos, Sov. Astron. Lett. **7**, 213 (1981).
[10] A. Gould, Astrophys. J. **386**, L5 (1992).
[11] A. Gould, Astron. Soc. Pac. Conf. Ser. **239**, 3 (2001)
[12] E. W. Kolb and I. I. Tkachev, Astrophys. J. **460**, L25 (1996).
[13] C. S. Kochanek, P. Schneider, and J. Wanbsganss, in *Part 2 of Gravitational Lensing: Strong, Weak and Micro, Proceedings of the 33rd Saas-Fee Advanced Course*, edited by G. Meylan, P. Jetzer, and P. North (Springer-Verlag, Berlin, 2004).
[14] M. Fukugita, T. Futamase, M. Kasai, and E. L. Turner, Astrophys. J. **393**, 3 (1992).
[15] C. C. Dyer and R. C. Roeder, Astrophys. J. **180**, L31 (1973).
[16] P. Schneider, J. Ehlers, and E. E. Falco, *Gravitational Lenses* (Springer-Verlag, New York, 1992).
[17] C. Meegan *et al.*, Astrophys. J. **702**, 791 (2009).
[18] D. Gruber *et al.*, Astron. Astrophys. **531**, A20 (2011).
[19] http://gcn.gsfc.nasa.gov.
[20] http://fermi.gsfc.nasa.gov/ssc/.
[21] A. Goldstein *et al.*, Astrophys. J. Suppl. Ser. **199**, 19 (2012).
[22] J. R. Mattox *et al.*, Astrophys. J. **461**, 396 (1996).
[23] M. A. Abramowicz, J. K. Becker, P. L. Biermann, A. Garzilli, F. Johansson, and L. Qian, Astrophys. J. **705**, 659 (2009).
[24] G. F. Marani, R. J. Nemiroff, J. P. Norris, K. Hurley, and J. T. Bonnell, Astrophys. J. Lett. **512**, L13 (1999).
[25] M. S. Briggs, D. L. Band, R. D. Preece, G. N. Pendleton, W. S. Paciesas, and J. L. Matteson, AIP Conf. Proc. **428**, 299 (1998).